Turbulence modeling of axisymmetric flow inside rotating cavities

H. Iacovides and I. P. Theofanopoulos
University of Manchester Institute of Science and Technology, Manchester, UK

This work examines the turbulence modeling problems present in the numerical computation of axisymmetric incompressible, isothermal flows through rotating cavities. More specifically it investigates flows in co-rotating disc geometries with radial inlet throughflow and enclosed disc flows with and without throughflow. A zonal turbulence modeling approach is adopted. In the fully turbulent region that covers most of the flow domain both the usual k–ε eddy–viscosity and the algebraic stress models (ASM) were tested. In the thin viscosity dominated wall regions two different versions of the mixing length hypothesis were employed. Comparisons with experimental measurements revealed that in all the cases examined in this study the key to the correct prediction of such flows lies in the proper modeling of the near-wall regions. For every test case examined, satisfactory predictions were obtained with at least one form of turbulence model. However, no single form was satisfactory in all cases and, indeed, of the forms tested, none proved to be distinctly superior to the others.

Keywords: flow computation; turbulence; rotating cavities

Introduction

The problem of flow in rotating disc cavities is of considerable importance to the design of gas turbine engines. In some cases both the two adjacent discs rotate, giving rise to the co-rotating disc system (Figure 1a). In another commonly encountered situation one of the discs forming the cavity is stationary creating a rotor–stator system, referred to in this study as an enclosed disc system (Figures 1b and 1c). Blade cooling requirements of advanced gas turbines sometimes necessitate the radial throughflow of relatively cool air in these systems, which is extracted from the compressor stages of the engine.

The real gas turbine disc cavities are of a complex three-dimensional (3-D) geometry and rotational buoyancy effects are also expected to be present. Most studies so far, however, have examined the idealized cases of axisymmetric cylindrical cavities. The earliest studies in this field (such as Von Karman's[1] and Cochran's[2]) considered theoretically the free disc problem and produced analytical solutions. The first sets of detailed hydrodynamic measurements on rotating cavity flows were perhaps provided by Daily and Nece[3] and Daily *et al.*[4] They examined enclosed disc systems with and without throughflow. Most of the subsequent progress in this field has been achieved through the efforts of the University of Sussex research group on both the experimental and the theoretical side. Owen and Pincombe,[5] Pincombe[6] and Owen *et al.*[7] concentrated on the problem of co-rotating disc flow. Detailed measurements and also analytical solutions were provided for a number of different throughflow conditions and under both laminar and turbulent flow regimes.

In the case of enclosed disc flows, these studies have shown that the variation in centrifugal force across the cavity gives rise to a recirculating flow pattern. Fluid in the vicinity of the rotating disc moves radially outward and returns radially inward along the stator surface. For the co-rotating disc case with radial outlet it has been shown that two Ekman layers are formed along the disc surfaces, which absorb all the radially moving fluid (Figure 2). This is caused by the presence of the radial motion and the interaction between the centrifugal and viscous forces. A more detailed explanation can be found in Owen *et al.*[7] Two dimensionless parameters that may be used to characterize these flows are the mass flow rate coefficient C_w and the rotational Reynolds number Re_θ. They are defined as:

$$C_w = \frac{m'}{\mu b} \quad \text{and} \quad \mathrm{Re}_\theta = \frac{\Omega b^2}{\nu}$$

where m' is the mass flow rate, b the maximum length of the geometry and Ω the disc angular velocity.

Even though analytical methods have been applied to some of these rotating cavity flows with a fair degree of success, the development of reliable numerical predictive methods would be of a wider practical value. The finite difference computations of Chew *et al.*[8] for laminar co-rotating disc flow have proved that once the considerable stability problems are overcome numerical methods can correctly predict the laminar flow case.

As far as turbulent flow predictions are concerned, the evidence is less conclusive. Chew[9] computed turbulent co-rotating disc flows using the high Reynolds number version of the k–ε turbulent model with the "wall function" approximation accounting for the near-wall effects on turbulence (k–ε–WF). This modeling arrangement failed to mimic major characteristics of the flow. Surprisingly, the subsequent application of the mixing length model (ML), Chew[10,11] and Chew and Vaughan,[12] resulted in predictions that were closer to the experimental data for the co-rotating disc case and to satisfactory predictions for the enclosed disc flows. Morse[13] applied the Launder and Sharma[14] low Reynolds number version of the k–ε model (k–ε–LR). This version, in common with the mixing length model, has no need for the use of the wall function approximation. The application of k–ε–LR resulted in considerable improvements in the predictions over Chew's earlier k–ε–WF computations. Morse, however, reported that this model displayed a tendency to laminarize the flow under conditions that are known to be turbulent. Another application

Address reprint requests to Dr. Iacovides at the University of Manchester Institute of Science and Technology, Manchester M60 1QD, UK.

Received 1 June 1989; accepted 23 July 1990

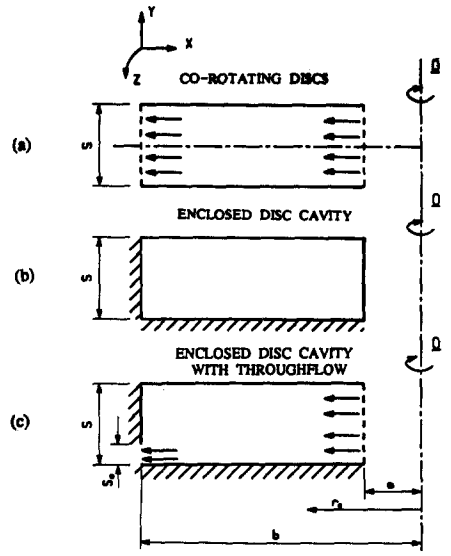

Figure 1 Coordinate systems

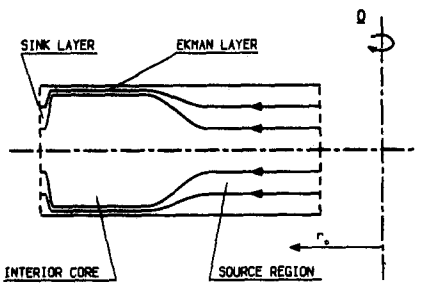

Figure 2 Co-rotating discs; flow structure

of a low Reynolds number k–ε model is that of Louis and Salhi.[15] They applied the Lam and Bremhorst[16] version (a somewhat less general version than that of Launder and Sharma) to the co-rotating disc case. Their predictions were in agreement with Pincombe's data, but the study was limited to Re_θ values of up to 10^5.

These numerical studies seem to indicate that the use of the wall function approximation is not appropriate in the case of rotating disc flows where 3-D boundary layers are present. Recent work on 3-D flow in curved ducts by Choi *et al.*[17] has also resulted in similar conclusions. A more precise analysis of the dynamics of the near-wall region is thus necessary. The work of Morse on the other hand indicates that the low Reynolds number version of the k–ε model is still in need of further development. This has also been the conclusion of other researchers (Yap[18]). In any case the prohibitively fine grids required by the k–ε–LR model make it desirable to seek computationally less expensive modeling alternatives. The work done so far indicates that the mixing length model may be a suitable compromise. In more complex (and also more realistic) rotating disc flows, however, the influence of the near-wall region is not likely to be as dominant as in the cases examined so far. In such flow cases the use of a turbulence model based on transport equations would be more appropriate.

The present work, therefore, aims to explore the modeling alternatives in this direction. Earlier work on 3-D flows within our research group has proved that a zonal approach to modeling can offer an attractive compromise between accuracy and computational economy (Azzola *et al.*[19]; Choi *et al.*[17]). The solution domain is divided into two regions: the fully turbulent region, which occupies the greatest part of the flow domain, and the viscosity dominated region across the wall sublayers, which accounts for only a small fraction of the entire flow domain. A high Reynolds number model based on the

Notation

a	Disc inner radius
b	Disc outer radius
$C_1, C_2, C'_1, C'_2, C_{\varepsilon 1}, C_{\varepsilon 2}, C_{k_1}, C_{k_2}, C_k, C_\varepsilon, C_\mu, C_l$	Turbulent modeling constants
C_w	Mass flow rate coefficient, $m'/(\mu b)$
C_{mo}	Moment coefficient, $2M/(\rho\Omega^2 b^5)$
D	Mixing length model damping function
k	Turbulent kinetic energy
l_m	Turbulent length scale
M	Rotational moment
m'	Throughflow mass flow rate
n	Turbulence damping index
n_q	Unit vector normal to the wall
P	Pressure
P_k	Turbulent kinetic energy generation rate
P_{ij}	Generation rate for turbulent stress $\overline{u_i u_j}$
Re_θ	Rotational Reynolds number, $\Omega b^2/\nu$
r_c	Local radius of curvature, $b-x$
s	Disc spacing
U_T	Friction velocity, $\sqrt{\tau_w/\rho}$
U_i	Mean velocity vector
u_i	Fluctuating velocity vector
U	Mean velocity in radial direction
u	Radial velocity fluctuation
$\overline{u_i u_i}$	Turbulent stress tensor
V	Mean velocity in axial direction
v	Axial direction fluctuation
W	Mean velocity in circumferential direction
w	Circumferential velocity fluctuation
x	Radial direction
Y	Distance normal to the wall
y	Axial direction
y^+	Dimensionless wall distance, YU_T/ν
Z	Circumferential direction

Greek symbols

δ_{ij}	Kronecker delta
ε	Turbulent kinetic energy dissipation rate
ε_{ijk}	Third-order alternating tensor
κ	Von-Karman's constant
μ	Dynamic viscosity
μ_t	Turbulent viscosity
ν	Kinematic viscosity
ρ	Density
σ	Turbulent Prandtl number
τ	Local shear stress
τ_w	Wall shear stress
Φ^w_{ij}	Wall reflection term
Ψ	General scalar variable
Ω	Angular velocity of rotation

transport of turbulence quantities such as the k–ε can then be employed in the fully turbulent region with a simpler low Reynolds number model in the near-wall regions such as the van-Driest[20] mixing length model. One added advantage of this modeling approach is that the model in the two different zones can be changed independently, thus providing a clearer assessment of the relative influence of the two regions on the overall flow structure.

With this in mind during the course of the present study, it was decided to use two different models of the two zones leading to a total of four different turbulence modeling arrangements. In the near-wall regions two different versions of the mixing length model were employed. The van-Driest[20] version and one proposed by Koosinlin *et al.*[21] subsequently referred to as ML1 and ML2, respectively. The former version has been successfully applied, within the zonal modeling approach, to rotating pipe flows (Iacovides and Launder[22]), and the latter had been specifically developed for flow over rotating discs and cones. In the fully turbulent region, as well as the standard k–ε effective viscosity model of Jones and Launder,[23] an algebraic stress model (ASM) was also employed. The use of the ASM model provides for the first time the opportunity to evaluate the effects of anisotropic turbulence (in the fully turbulent region) on the overall flow structure.

In an attempt to arrive at conclusions of a more general nature, both co-rotating and enclosed disc flows were examined. The current predictions are compared with available experimental data and also with the numerical predictions of earlier studies.

Mathematical model

A rotating cylindrical coordinate system has been employed in this study as shown in Figure 1. The radial, axial, and circumferential directions are denoted by x, y, and z, respectively, with U, V, and W the corresponding velocity components. The local radius of curvature, which in this case is also the distance from the axis of rotation, is denoted by $r_c = b - x$.

Mean flow equations

The equations of mean motion are as follows:

- Continuity

$$\frac{1}{r_c}\left\{\frac{\partial}{\partial x}(\rho r_c U)+\frac{\partial}{\partial y}(\rho r_c V)\right\}=0$$

- Mean Momentum

$$\frac{1}{r_c}\left\{\frac{\partial}{\partial x}(\rho r_c U\Psi)+\frac{\partial}{\partial y}(\rho r_c V\Psi)\right\}=\frac{1}{r_c}\left\{\frac{\partial}{\partial x}\left[r_c\mu\frac{\partial\Psi}{\partial x}-r_c\rho\overline{u\Psi}\right]+\frac{\partial}{\partial y}\left[r_c\mu\frac{\partial\Psi}{\partial y}-r_c\rho\overline{v\Psi}\right]\right\}+S_P(\Psi)+S_D(\Psi)+S_C(\Psi)+S_R(\Psi)+S_{COR}(\Psi)+S_{CEN}(\Psi)$$

In this general version Ψ denotes U, V, or W; S_P represents the pressure gradient effects and S_C, S_D, and S_R the polar coordinate effects. Their expressions are given in Table 1.

S_{COR} and S_{CEN} represent the Coriolis and the centrifugal forces due to the rotation of the coordinate system. They are given in Table 2.

Turbulent stresses

In the case of the ASM model the turbulent stresses are obtained from separate algebraic expressions given here in Cartesian tensor notation:

$$\frac{\overline{u_iu_j}}{k}=\tfrac{2}{3}\delta_{ij}+\frac{(1-c_2)}{\varepsilon(c_1-1+P_k/\varepsilon)}\{P_{ij}-\tfrac{2}{3}P_k\delta_{ij}\}+\frac{\varphi^w_{ij}}{\varepsilon(c_1-1+P_k/\varepsilon)}$$

P_k is the turbulent kinetic energy generation rate term expressed as

$$P_k=-\overline{u_iu_j}\frac{\partial U_i}{\partial x_j}$$

P_{ij} is the generation rate term for the individual turbulent stress $\overline{u_iu_j}$:

$$P_{ij}=-\overline{u_iu_k}\frac{\partial U_j}{\partial x_k}-\overline{u_ju_k}\frac{\partial U_i}{\partial x_k}-2\Omega_p(\varepsilon_{ipq}\overline{u_qu_j}+\varepsilon_{jpq}\overline{u_qu_i})$$

φ^w_{ij} accounts for the wall reflection effects on the turbulent stresses:

$$\varphi^w_{ij}=\left[c'_1\frac{\varepsilon}{k}(\overline{u_qu_m}n_qn_m\delta_{ij}-\tfrac{3}{2}\overline{u_iu_q}n_qn_j-\tfrac{3}{2}\overline{u_ju_q}n_in_q)+c'_2(\varphi_{qm_2}n_qn_m\delta_{ij}-\tfrac{3}{2}\varphi_{qi_2}n_qn_j-\tfrac{3}{2}\varphi_{qj_2}n_in_q)\right]f\left(\frac{l}{n_qY}\right)$$

$$\varphi_{ij_2}=-c_2(P_{ij}-\tfrac{2}{3}P_k\delta_{ij})$$

n_q is the unit vector normal to the wall, Y the distance from the wall to the point in question, and l the local turbulent length scale defined as

$$l=\frac{k^{3/2}}{C_l\varepsilon}$$

The function $F(l/n_qY)$ has the following expressions for the x and y directions:

$$F(l/n_xY)=\frac{l}{x}+\frac{l}{(b-a)-x}$$

$$F(l/n_xY)=\frac{l}{x}+\frac{l}{s-y}$$

In the k–ε and also in the mixing length models used in this work, the turbulent stresses are obtained from the effective viscosity approximation:

$$\rho\overline{u_iu_j}=\tfrac{2}{3}\rho k\delta_{ij}-\mu_t\left(\frac{\partial U_i}{\partial x_j}-\frac{\partial U_j}{\partial x_i}\right)$$

In the k–ε model the effective viscosity μ_t is an algebraic function of the turbulent kinetic energy k and its dissipation

Table 1

Ψ	U	V	W
$S_P(\Phi)$	$-\partial p/\partial x$	$-\partial p/\partial y$	0
$S_C(\Psi)$	$-\rho W^2/r_c$	0	$\rho UW/r_c$
$S_D(\Psi)$	$-2\mu U/r_c^2$	0	$-\mu W/r_c^2$
$S_R(\Psi)$	$-\rho w^2/r_c$	0	$\rho\overline{uw}/r_c$

Table 2

Ψ	U	V	W
$S_{COR}(\Psi)$	$2\sigma\Omega W$	0	$-2\rho\Omega U$
$S_{CEN}(\Psi)$	$\rho r_c\Omega^2$	0	0

rate ε:

$$\mu_t=\frac{\rho c_\mu k^2}{\varepsilon}$$

In the case of the mixing length models,

$$\mu_t=\rho l_m^2\left\{\frac{\partial U_i}{\partial x_j}\left(\frac{\partial U_i}{\partial x_j}+\frac{\partial U_j}{\partial x_i}\right)\right\}^{1/2}$$

The mixing length scale l_m at the near wall regions is expressed as

$$l_m=\kappa y(1-\exp(-D))$$

For the van-Driest version (ML1), the damping function D depends on the wall friction velocity U_T:

$$D=\frac{YU_T}{26\nu}$$

In the version proposed by Koosinlin *et al.* (ML2), the local shear stress τ acting on a surface parallel to the wall is also included in the damping term:

$$D=\frac{YU_T(\tau/\tau_w)^n}{26\nu}$$

The recommended value for n is 1.5.

k and ε transport equations

These quantities are required by both the ASM and the k–ε models. They are obtained from separate transport equations.

When the ASM model is used, these equations adopt the following form:

$$\frac{1}{r_c}\left\{\frac{\partial}{\partial x}(\rho r_c U\Psi)+\frac{\partial}{\partial y}(\rho r_c V\Psi)\right\}$$
$$=\frac{1}{r_c}\left\{\frac{\partial}{\partial x}\left[r_c\left(\mu+\rho C_\Psi\frac{k}{\varepsilon}\overline{u^2}\right)\frac{\partial\Psi}{\partial x}+r_c\rho C_\Psi\frac{k}{\varepsilon}\overline{uv}\frac{\partial\Psi}{\partial y}\right]\right.$$
$$\left.+\frac{\partial}{\partial y}\left[r_c\left(\mu+\rho C_\Psi\frac{k}{\varepsilon}\overline{v^2}\right)\frac{\partial\Psi}{\partial y}+r_c\rho C_\Psi\frac{k}{\varepsilon}\overline{uv}\frac{\partial\Psi}{\partial y}\right]\right\}$$
$$+C_{\Psi_1}\rho\frac{\Psi}{k}P_k-C_{\Psi_2}\rho\frac{\Psi}{k}\varepsilon$$

where Ψ can be either k or ε.

In the k–ε model the equations are somewhat simpler:

$$\frac{1}{r_c}\left\{\frac{\partial}{\partial x}(\rho r_c U\Psi)+\frac{\partial}{\partial y}(\rho r_c V\Psi)\right\}=\frac{1}{r_c}\left\{\frac{\partial}{\partial x}\left[r_c\left(\mu+\frac{\mu_t}{\sigma_\Psi}\right)\frac{\partial\Psi}{\partial x}\right]\right.$$
$$\left.+\frac{\partial}{\partial y}\left[r_c\left(\mu+\frac{\mu_t}{\sigma_\Psi}\right)\frac{\partial\Psi}{\partial y}\right]\right\}+C_{\Psi_1}\rho\frac{\Psi}{k}P_k-C_{\Psi_2}\frac{\Psi}{k}\varepsilon$$

The values of the constants appearing in the turbulence modeling equations are given in Table 3.

Numerical aspects

The numerical solver employed in this investigation is a finite difference control volume procedure, originating from the TEACH family of codes. Having been earlier applied to 3-D turbulent flows (Iacovides and Launder[24]), it was subsequently simplified to a two dimensional (2-D) solver with three velocity components.

The inclusion of Leonard's[25] QUICK scheme for the discretization of convection of momentum and the employment of Patankar's[26] SIMPLER algorithm for the solution of the pressure field are two of the nonstandard TEACH options incorporated in this code. The initial use of QUICK[25] for the co-rotating disc flows resulted in predictions identical to those obtained using HYBRID[27] with the same grid density. This is probably because over most of the flow domain the flow streamlines are parallel to the grid lines. This reduces numerical diffusion even at high Peclet numbers. The HYBRID scheme was thus used in the subsequent computations. In the ASM version a number of extra stabilization measures were necessary. These include the staggering of the turbulent stresses, the use of the apparent viscosity concept, the iterative solution of the stress equations, and a special treatment of the generation rate term. These measures are explained in greater detail by Iacovides and Launder.[24]

As far as the co-rotating disc case boundary conditions are concerned, due to the use of a rotating co-ordinate system the circumferential velocity component W was set to zero at the rotating walls. Because of flow symmetry only half the flow domain was considered with symmetry boundary conditions along the line $y=0$ (Figure 1a). The radial component U was assumed to be axially uniform at outlet and inlet ($x=0$ and $x=b-a$). The values were determined from the overall mass balance:

$$\text{at } x=0,\ U=-\frac{m'}{2\pi\rho bs};\qquad \text{at } x=b-a,\ U=-\frac{m'}{2\pi\rho as}$$

For the enclosed disc computations the W component at the stationary surfaces was set to $-\Omega r_c$. In the throughflow situation, axially uniform U velocity again was assumed at the entry boundary and at the exit slot.

Due to the use of the mixing length model in the wall regions no special treatment was needed for the turbulent quantities at the wall boundaries. Boundary values for the turbulence quantities do, however, need to be specified at the interface between the two modeling zones. k and ε are prescribed by assuming local equilibrium ($P_k=\varepsilon$) and continuity of effective viscosity ($l_m^2\sqrt{P_k}/\nu_t=c_\mu k^2/\varepsilon$) in the mixing length region node adjacent to the interface. The boundary turbulent stresses can then be obtained through the effective viscosity approximation. The determination of the mixing length region thickness is based on the dimensionless distance from the wall. The value of y^+ ($=U_TY/\nu$) along the interface was kept between 60 and 100 in all cases. It was also important that the y^+ value of the nodes adjacent to the wall was less than 3. This ensures that the

Table 3

C_1	C_2	C_1'	C_2'	$C_{\varepsilon 1}$	$C_{\varepsilon 2}$	C_{k1}	C_{k2}	C_k	C_ε	C_μ
1.8	0.6	0.5	0.3	1.44	1.92	1	1	0.22	0.15	0.09

C_l	σ_k	σ_ε	κ
2.55	1	1.22	0.42

Table 4

Geom.	Co-rotating discs		Enclosed discs		
Re_θ	10^5	4×10^5	6.9×10^5	6.9×10^5	4.4×10^6
C_w	1092	1092	0	3795	0
s/b	0.1333	0.1333	0.0685	0.0685	0.0255
a/b	0.1	0.1	0.11	0.11	0.1
Case	I	II	III	IV	V
Present study models	k–ε–ML1 k–ε–ML2 ASM—ML1 ASM—ML2		k–ε–ML1 k–ε–ML2 ASM—ML1 ASM—ML2		k–ε–ML1 ASM—ML1
Earlier studies	k–ε–WF (Chew[19]) ML (Chew[10]) k–ε–LR (Morse[13])		ML (Chew and Vaughan[12])		ML (Chew and Vaughan[12])
Expt. data	Pincombe[6]		Daily *et al.*[4]		Daily and Nece[3]

near-wall node is located within the viscosity dominated part of the sublayer.

Finally, the question of numerical uncertainty was also considered. A number of different grid sizes and grid distributions were tested so as to ensure that the predictions were free of significant numerical errors. In co-rotating disc flows a 45 by 45 nonuniform mesh was found to be adequate, having resulted in predictions identical to those obtained with a 61 by 61 mesh. For the enclosed dsic predictions 51 by 81 (axial by radial) nonuniformly distributed nodes were employed for the aspect ratio of 0.0255. These nonuniform grid arrangements, which are of similar density to the ones applied by Chew and Vaughan,[12] are believed to be fine enough to produce solutions with a negligible degree of grid dependence. In all the computations about a third of the total number of nodes was located in the mixing length zones.

Results

The details of the investigated cases of this study, those of the earlier related computations, and also of the relevant experimental studies are given in Table 4.

Figure 3 provides a pictorial overview of all these cases through a set of axial plane velocity vector plots and, for the rotating disc flows, tangential velocity contour plots. The arrows indicate the axial traverse lines along which experimental measurements have been obtained. In the case of co-rotating discs the measurements include only the radial velocity component, whereas, in the enclosed discs, the tangential velocity was also recorded along the indicated traverse lines. The co-rotating disc cases measurements of the tangential velocity are available only at two locations along the symmetry line. Comparison between current predictions and available experimental and numerical data is divided into two parts, one concerned with the two co-rotating disc flow cases and one examining the flow behaviour in enclosed disc systems.

Co-rotating disc flows (Cases I and II)

The formation of the Ekman Layers can be clearly seen in Figure 3, Cases I and II. It is also fairly evident that as the value of Re_θ is increased the Ekman-layer region occupies a greater proportion of the cavity and the boundary-layer thickness is reduced. In both cases the radial velocity traverse line is located within the Ekman-layer region. The detailed comparisons are shown in Figure 4.

In Case I, where the rotational speed is lower ($Re_\theta = 10^5$), the radial velocity comparisons indicate that the use of ML1 in the wall regions results in the prediction of thicker boundary layers than the one experimentally observed. The introduction of the ASM model in the fully turbulent region instead of the k–ε does not produce any significant change in the predictions. The effects of near-wall modeling on the other hand are clearly visible. The introduction of ML2 (instead of ML1) leads to thinner predicted boundary layers and thus to predictions that are closer to the experimental data than the ones resulting from the use of either ML1 or wall function across the sublayer. The tangential velocity comparisons reinforce these conclusions. It therefore appears that, in order to produce realistic computations of this flow, it is necessary to simulate the reduction in the near-wall turbulent length scales, which is probably caused by the rapid change in the shear stress across the boundary layer.

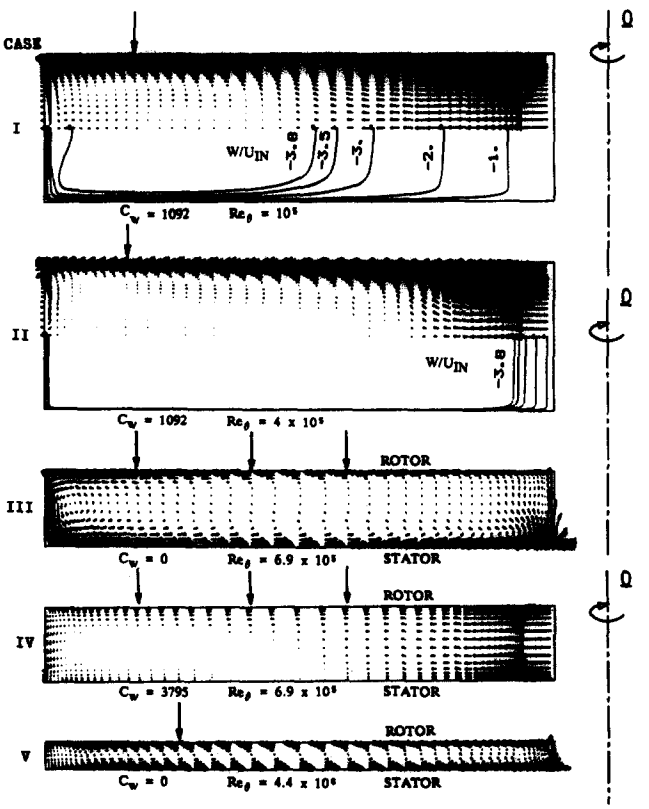

Figure 3 Predicted overall flow structure of the cases examined in the present study

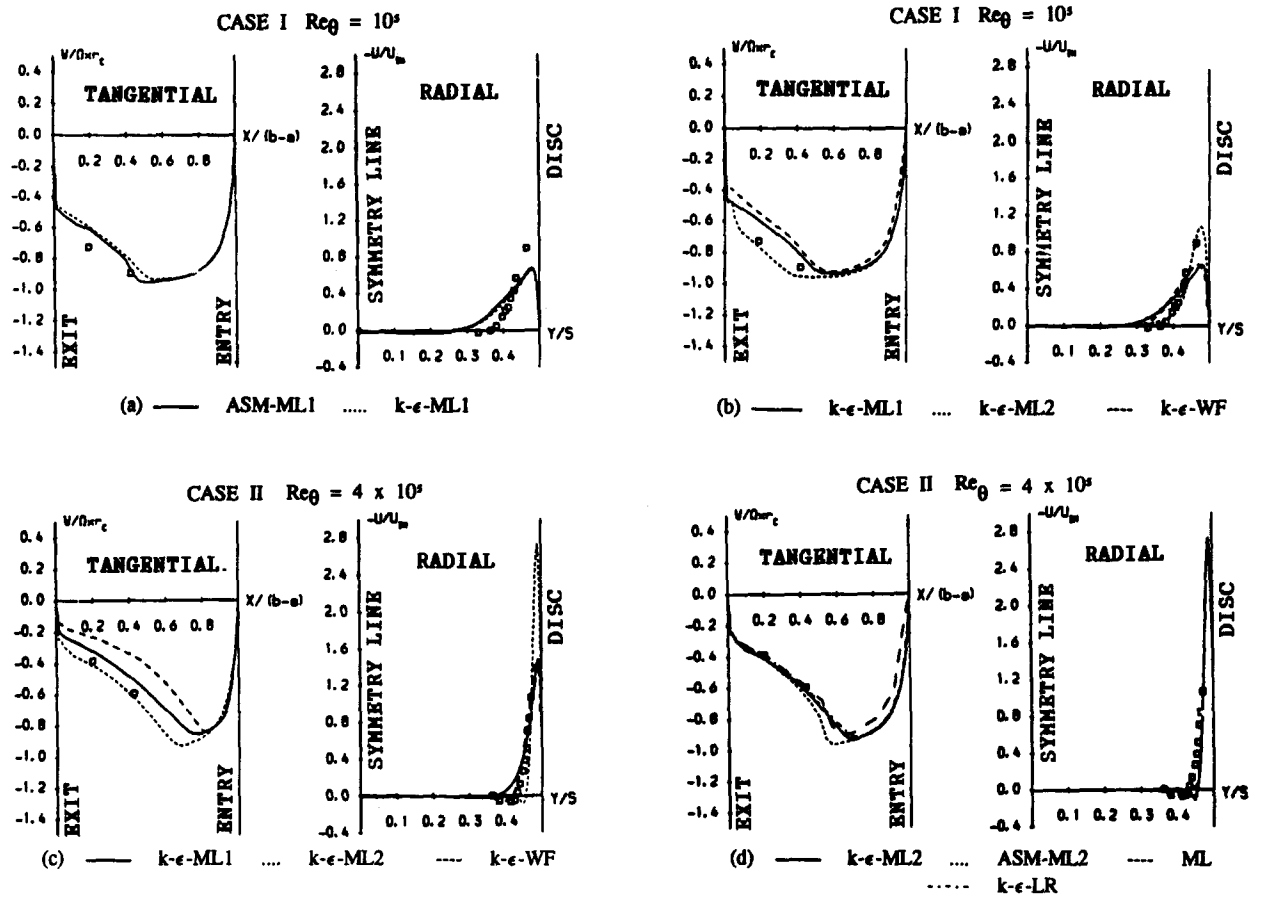

Figure 4 Co-rotating discs' flow mean velocity profile comparisons: $s/b=0.133$, $a/b=0.1$, $C_w=1092$, 0; Expt., Pincombe[6]

A similar overall turbulence modeling behavior is also present in the higher rotational speed comparisons of Case II at $Re_\theta=4\times10^5$. Even though boundary layers are considerably thinner, the near-wall modeling is still of crucial importance. Some rotation-related trends do emerge, however. The radial velocity comparisons indicate that the two ML2-based models and also k–ε–LR and ML appear to overpredict the extent of near-wall turbulence dissipation resulting in boundary layers that are somewhat thinner than the measured one. The ML1-based models on the other hand, in common with k–ε–WF, produce unrealistically thick boundary layers, which in turn lead to poorer tangential velocity predictions. The performance of k–ε–WF at this higher speed deteriorates even further in relation to all the other models. Another potentially significant trend is the fact that greater differences now begin to appear between the ASM and k–ε generated tangential velocity predictions. While these differences are still relatively small, they could be more substantial at engine operating rotational speeds, which are higher than the ones examined so far. The limited amount of experimental data, however, does not enable us to decide which of these two high Reynolds number models is more successful.

The main conclusion from the investigation of these two co-rotating disc flows is that the correct modeling of the near-wall turbulence is instrumental in producing realistic mean flow predictions. Because of the reduction of the near-wall turbulent length scales ML2 and k–ε–LR are found to be the most appropriate near-wall models of the ones applied so far. The modeling of the fully turbulent region is found to be less critical, but it does begin to become more important at higher rotational speeds.

Enclosed disc flows (Cases III, IV, and V)

The first case examined is that of the largest aspect ratio cavity without throughflow shown in Figure 3, Case III. The predictions reveal a radial flow recirculation pattern with a central core in which the radial velocity is almost zero. The velocity profile comparisons at three radial locations ($r_c/b=0.83$, 0.65, and 0.47) are presented in Figure 5. It should be noted that the near-wall turbulent length scale prescription in Chew and Vaughan's[12] ML computation is similar to that in ML2 but with the value of n set to 0.75 instead of the recommended 1.5. The radial velocity comparisons show that the use of ML2 now results in the prediction of radial velocity boundary layers, which, at the outer region of the cavity, are thinner than those indicated by the experimental data. The differences between the k–ε and ASM predictions are again very small. At the inner region the differences between the radial velocity predictions of the different models disappear and agreement with the experimental data is satisfactory. The tangential velocity comparisons seem to show that the ML1-based computations underpredict somewhat the core tangential velocity in the outer region and overpredict it in the inner region. In the case of the ASM model the introduction of ML2 led to some deterioration in the quality of the tangential velocity predictions. The use of ML1 near-wall model can be said to produce better overall predictions than ML2. The ML predictions appear to be in close agreement with the ML1 based predictions of the present study.

The failure of all the models to predict the tangential velocity at the first radial position ($r_c/b=0.47$) is probably due to the fact that the flow becomes laminar at lower radii. The models

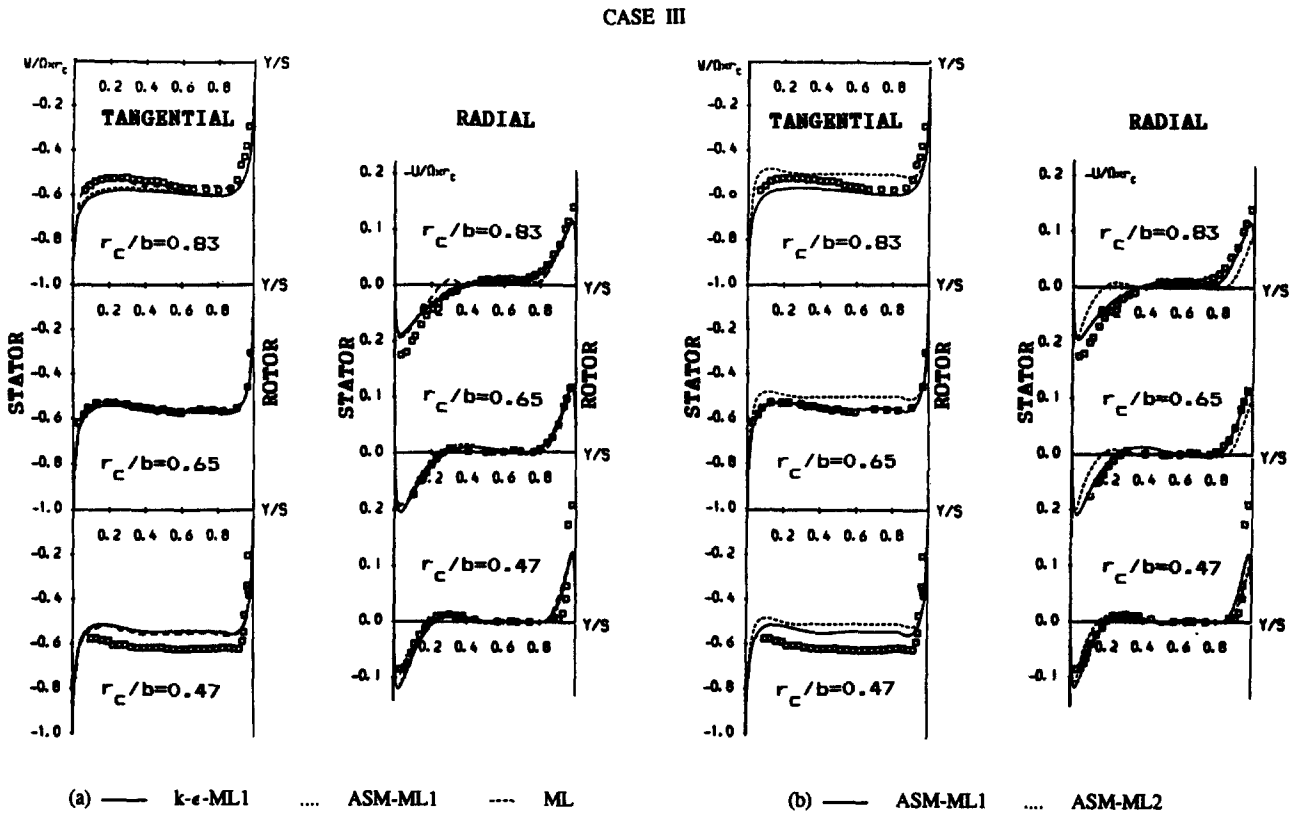

Figure 5 Mean velocity profile comparisons, Case III. Enclosed disc system without throughflow: $C_w=0$; $Re_\theta=6.9\times10^5$, $a/b=0.11$; $s/b=0.0685$, 0; Expt., Daily *et al.*[4]

employed in the present study are not able to predict this phenomenon. As shown in a recent buoyant cavity flow study by Ince and Launder[28] a low Reynolds number form of the two-equation model would need to be employed.

Another interesting comparison of practical importance for this case concerns the value of the moment coefficient Cm_0 defined as

$$Cm_0=\frac{2M}{\rho\Omega^2 b^5}$$

Table 5 compares the current predictions' Cm_0 values with Daily and Nece's[3] experimental one and also with those of Chew and Vaughan's[12] ML predictions. One of the two ML predictions was obtained using ML1. In the second ML prediction Chew and Vaughan[12] used the ML2 version, but for numerical stability the damping index n was given the nonstandard value of 0.75.

The strong influence of near-wall turbulence modeling is again clearly evident. The damping of the near-wall turbulent length scale appears to be the only determining factor in the prediction of the moment coefficient. Low damping ($n=0$) leads to unrealistically high values (by about 11%), and a damping value of 1.5 underpredicts the coefficient by about 11%. A value of 0.75 for n results in an intermediate predicted value of Cm_0, which is closer to the experimental value. The turbulence modeling of the fully turbulent region appears to have no effect on the moment coefficient prediction.

In Case IV the imposition of throughflow (at $C_w=3795$) results in major changes to both the flow itself (Figure 3, Case IV) and also to the relative behavior of the turbulence models. Most of the radial flow is squeezed into the vicinity of the rotor surface. In contrast to the no-throughflow case, away from the rotor most of the fluid is now non-rotating (Figures 5 and 6). The radial velocity profiles of Figure 6 show that there is now practically no difference between the ML1- and ML2-based radial velocity predictions. In the two outer locations these predictions manage to mimic very closely the experimental behavior. At these same two locations, ML produces unrealistic (albeit small) overshoots. Similar behavior was also exhibited by ML at the outermost traverse line in the Case III comparisons (no throughflow) in Figure 5. At the innermost traverse line ($r_c/b=0.47$) all predictions fail to reproduce the measured radial velocity distribution. There are also at this location substantial differences between the ASM and k–ε predictions. In the stator region the ASM and also the ML predictions are closer to the measurements. The failure of the predictions in the rotor region can be partly explained by the experimentally observed fact

Table 5

		Present study computations				Chew and Vaughan[12]	
Case III	Expt.	k–ε–ML1 $n=0$	ASM—ML1 $n=0$	k–ε–ML2 $n=1.5$	ASM—ML2 $n=1.5$	ML $n=0.75$	ML $n=0$
$Cm_0\times10^3$	2.752	3.077	3.033	2.456	2.451	2.912	3.059

CASE IV

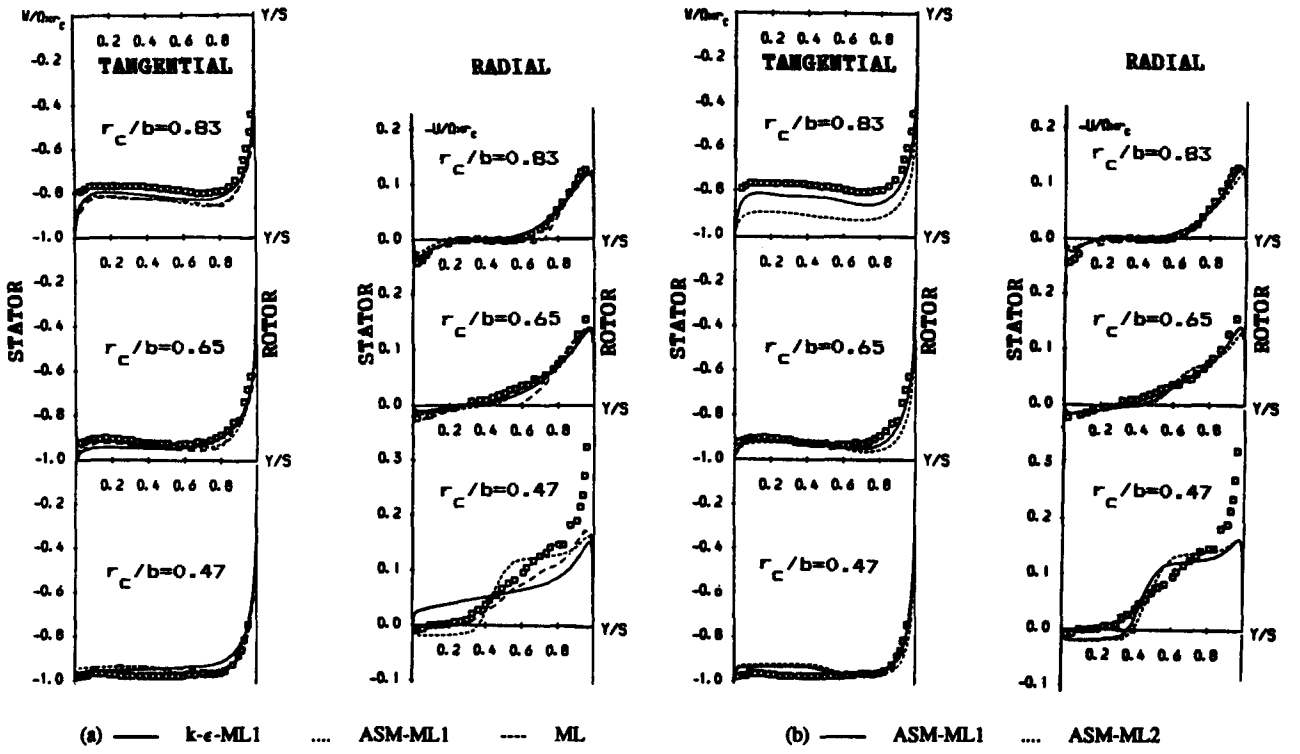

Figure 6 Mean velocity profile comparisons, Case IV. Enclosed disc system with throughflow: $C_w=3795$; $Re_\theta=6.9\times10^5$, $a/b=0.11$; $s/b=0.0685$, 0; Expt., Daily *et al.*[4]

that the flow becomes unstable in the inner region of the cavity, a phenomenon that cannot be taken into account by these computations. Another point worth noting, however, is that at this location ($r_c/b=0.47$) the measured radial flow rate seems to be higher than the predicted ones, whereas at the other two locations they appear to be the same.

The tangential velocity comparisons of Figure 6 show that the two ML1-based predictions and also ML are very close to the measurements. The introduction of ML2 at the wall sublayer leads to the deterioration of the tangential velocity predictions at the outermost radial velocity location. As in the other cases, the use of ASM in the fully turbulent region does not result in any significant changes in the predictions. Overall the comparisons show fewer differences between the various sets of predictions in the throughflow case (Case IV), but, as in the corresponding no-throughflow enclosed disc system (Case III), the two ML1-based predictions appear to be the more realistic.

The turbulent kinetic energy profiles of Figure 7 aim to provide a better understanding of the predictive behavior of the near-wall models in these two enclosed disc cases. As far as the predicted behavior is concerned, the most striking difference between Cases III and IV is the damping of turbulence along the stator surface, which is caused by the presence of throughflow. In both flows, the use of ML1 results in the prediction of higher turbulent kinetic energy levels than those of ML2. Also, in both cases the differences between the two sets of predictions tend to diminish at the inner region of the cylindrical cavity. The main distinguishing feature in the predictive behavior of the two near-wall models in these two flows is the fact that in the absence of throughflow, in Case III, there is a greater deviation between the two sets of turbulent kinetic energy predictions. This is of course consistent with the mean flow comparisons.

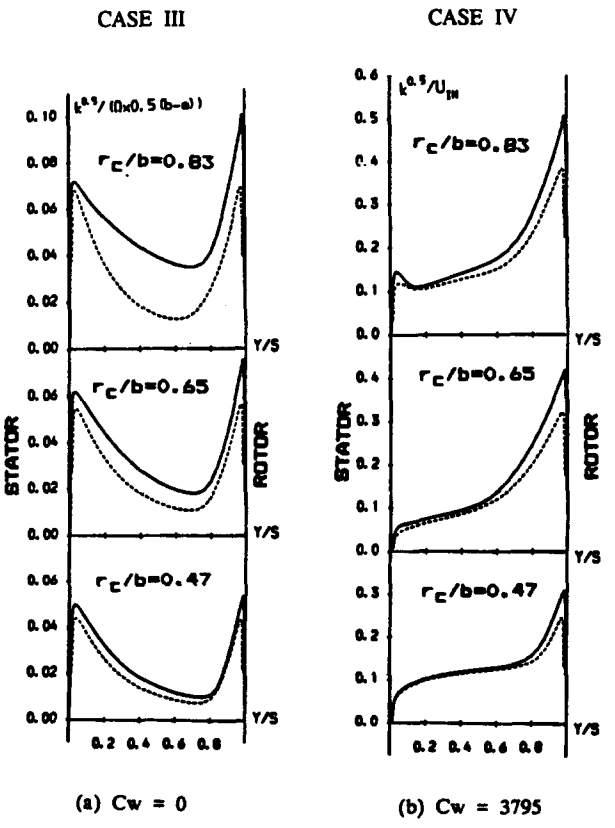

Figure 7 Turbulent kinetic energy comparisons for enclosed disc systems: $a/b=0.11$; $s/b=0.0685$; $Re_\theta=6.9\times10^5$; —— k–ε–ML1; ····· k–ε–ML2

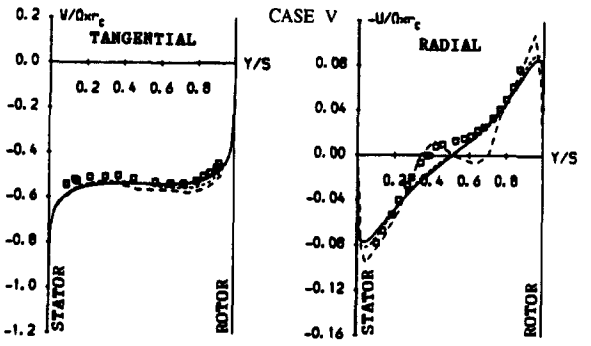

Figure 8 Mean velocity profile comparisons for enclosed disc flow, Case V: $a/b=0.1$; $s/b=0.0255$; $C_w=0$; $Re_\theta=4.4\times10^6$; $r_c/b=0.765$; —— k–ε–ML1; ····· ASM–ML1; ---- ML; 0; Expt., Daily and Nece[3]

Finally the enclosed disc system examined in Case V provides the opportunity to test the current models at a higher rotational speed ($Re_\theta=4.4\times10^6$) and a smaller aspect ratio ($s/b=0.0255$). Based on the conclusions of the two previous cases, only ML1-based predictions were carried out. The overall predicted flow field is shown in Figure 3, Case V. Unlike the larger aspect ratio case of Figure 3, Case III, there is no core region containing radially stationary fluid. Comparisons of velocity profiles along the indicated traverse line ($r_c/b=0.765$) are shown in Figure 8. The two present study models and ML produce similar and satisfactory predictions of the tangential velocity component. The radial velocity predictions, while still satisfactory, are not as close to the data as the tangential ones. The present study predictions fail to reproduce the plateau that appears in the measured profile in the middle of the cavity. The earlier ML predictions show two unrealistic overshoots in the same region. These observations are consistent with the ones made for the other two enclosed disc flows.

Conclusions

The strongest common characteristic in all the rotating cavity flows examined in this study is the fact that they are highly wall dominated. This is because the mean flow driving force results from the interaction between the rotation induced centrifugal forces and the viscosity dominated boundary layer regions. Furthermore, because none of the flows presented contained boundary-layer separation the modeling of the near-wall regions proved to be the critical factor for their correct prediction.

The zonal modeling approach adopted in this study, which carries the integration of momentum equations up to the wall, has been shown to be a cost-effective method of providing a suitable transport-based turbulence model. Predictions obtained using this method are in agreement with existing experimental data. The accuracy of the current predictions is at least comparable to that found in earlier studies. Neither of the two near-wall models examined in this study, however, appears to be universally successful in all the rotating disc flows. In co-rotating discs where there is strong damping of near-wall turbulence, ML2 is found to be more suitable, whereas in enclosed disc systems ML1 is better able to mimic the real flow. In co-rotating disc flows, as the rotational speed increases the sensitivity of the resulting predictions to the near-wall turbulence model does not appear to diminish. The use of a one equation k–l model such as Wolfshtein's[29] may prove to be a better compromise between cost effectiveness and consistency within the framework of transport-based modeling. This near-wall model should also be better able to cope with more complex rotating disc flows which may include 3-D effects and boundary-layer separation.

The comparisons of this study imply that the modeling of the fully turbulent region is of marginal importance to rotating disc flows. Nevertheless, in the case of co-rotating discs the fully turbulent region modeling displayed a tendency to become more significant at higher rotational speeds. This trend together with the requirement to be able to examine more complex rotating cavity flows suggests that the use of a nonisotropic model may become necessary in the investigation of more practically relevant cases.

Acknowledgments

The authors wish to thank Professor B. E. Launder, head of the Thermo and Fluids Division at UMIST, for his advice and encouragement. The research described herein has been undertaken for Rolls-Royce plc. Their support and the constructive comments and advice of Dr. John Chew of Rolls-Royce, Derby, are gratefully acknowledged. The manuscript has been prepared by Mrs. I. Bowker. Authors' names appear alphabetically.

References

1 Von-Karman, T. Uber Laminaire und Turbulente Reibung. *Z. Agnew Meth. Mech.*, 1921, **1**, 233
2 Cochran, W. G. The flow due to a rotating disc. *Proc. Cambridge Phil. Soc.*, 1934, **30**, 365
3 Daily, J. W. and Nece, R. E. Chamber dimension effects on induced flow and frictional resistance of enclosed rotating discs. *ASME J. Basic Engr.*, 1960, **82**, 217
4 Daily, J. W., Ernst, W. D., and Asbedian, V. V. Enclosed rotating discs with superposed throughflow; Mean steady and periodic unsteady characteristics of induced flow. Report No. 64, Hydrodynamic Lab., MIT, 1964
5 Owen, J. M. and Pincombe, J. R. Velocity measurements inside a rotating cylindrical cavity with a radial outflow of fluid. *JFM*, 1980, **99**, 111
6 Pincombe, J. R. Velocity measurements in the MK II-rotating cavity rig with a radial outflow. Report No. TFMRC/21, School of Engineering and Applied Sciences, University of Sussex, 1981
7 Owen, J. M., Pincombe, J. R., and Rogers, R. H. Source-sink flow inside a rotating cylindrical cavity. *JFM*, 1985, **155**, 233
8 Chew, J. W., Owen, J. M., and Pincombe, J. R. Numerical predictions for laminar source-sink flow in a rotating cylindrical cavity. *JFM*, 1984, **143**, 451
9 Chew, J. W. Prediction of flow in rotating disc systems using the k–ε turbulence model. ASME, 84-GT-229, Gas Turbine Conf., Amsterdam, 1984
10 Chew, J. W. Prediction of flow in a rotating cavity with radial outflow using a mixing length turbulence model. *Proc. Conf. on Num. Meth. in Lam. and Turb. Flow*, Swansea 1985, Pineridge Press, 318
11 Chew, J. W. Computation of flow and heat transfer in rotating disc systems. *Proc. 2nd ASME–JSME Therm. Engr. Conf.*, vol. 3, 1987, 361
12 Chew, J. W. and Vaughan, C. M. Numerical predictions of the flow induced by an enclosed rotating disc. ASME, 88-GT-127, Gas Turbine and Aeroengine Cong., 1988, Amsterdam
13 Morse, A. P. Numerical prediction of turbulent flow in rotating cavities. ASME, 87-GT-74, Gas Turbine Conf. and Ex., Anaheim, California, USA, 1987
14 Launder, B. E. and Sharma, B. I. Application of the energy-dissipation model of turbulence to the calculation of flow near a spinning disc. *J. Heat and Mass Transfer*, 1974, **1**, 131
15 Louis, J. F. and Salhi, A. Turbulent flow velocity between co-axial discs of finite radius. ASME 88-GT-47, Gas Turbine and Aeroengine Exp., Amsterdam, 1988
16 Lam, C. K. G. and Bremhorst, K. A. Modified form of the k–ε model for predicting wall turbulence. *J. Fluids Eng.* 1981, **103**

17 Choi, Y. D., Iacovides, H., and Launder, B. E. Numerical computation of turbulent flow in a square-sectioned 180 deg. bend. *J. Fluids Engr.* 1989, **111**, 59

19 Yap, C. R. Turbulent heat and momentum transfer of re-circulating and impinging flows. Ph.D. Thesis, University of Manchester, Faculty of Technology, 1987

19 Azzola, J., Humphrey, J. A. C., Iacovides, H., and Launder, B. E. Developing turbulent flow in a U-bend of circular cross-section: Measurement and computation. *J. Fluids Eng.* 1986, **180**, 214

20 Van-Driest, E. R. On turbulent flow near a wall. *J. Aero. Soc.*, 1956, **23**, 1007

21 Koosinlin, M. L., Launder, B. E., and Sharma, B. I. Prediction of momentum heat and mass transfer in swirling turbulent boundary layers. *J. Heat Transfer*, 1974, **98**, 204

22 Iacovides, H. and Launder, B. E. Numerical simulation of flow and heat transfer in tubes in orthogonal-mode rotation. *Proc. 6th Symp. on Turb. Shear Flows*, Toulouse, 1987

23 Jones, W. P. and Launder, B. E. The prediction of laminarization with a two equation model of turbulence. *Int. J. Heat Mass Transfer*, 1972, **15**, 301

24 Iacovides, H. and Launder, B. E. ASM predictions of turbulent momentum and heat transfer in coils and U-bends. *Proc. 4th Int. Conf. on Num. Meth. in Lam. and Turb. Flows*, 1985, Pineridge Press, Swansea, 1023

25 Leonard, B. P. A stable and accurate convective modelling procedure based on a quadratic upstream interpretation. *Comp. Meth. Appl. Engr.*, 1979, **19**, 59

26 Patankar, S. V. *Numerical Heat Transfer and Fluid Flow.* McGraw-Hill, New York, 1980

27 Spalding, D. B. A novel finite-difference formulation for differential expressions involving both first and second derivatives. *Int. J. Num. Meths. Engr.*, 1970, **4**, 551

28 Ince, N. Z. and Launder, B. E. On the computation of buoyancy-driven turbulent flows in rectangular enclosures. *Int. J. Heat and Fluid Flow*, 1989, **10**(2), 110

29 Wolfshtein, M. The velocity and temperature distribution in one-dimensional flow with turbulence augmentation and pressure gradient. *Int. J. Heat and Mass Transfer*, 1969, **12**, 301